

Nonlinear analysis of composite beams with partial shear interaction by means of the direct stiffness method

G. Ranzi*

The University of Sydney, NSW 2006, Australia

M.A. Bradford

The University of New South Wales, UNSW, Sydney, NSW 2052, Australia

(Received October 24, 2006, Accepted December 17, 2008)

Abstract This paper presents a modelling technique for the nonlinear analysis of composite steel-concrete beams with partial shear interaction. It extends the applicability of two stiffness elements previously derived by the authors using the direct stiffness method, i.e. the 6DOF and the 8DOF elements, to account for material nonlinearities. The freedoms are the vertical displacement, the rotation and the slip at both ends for the 6DOF stiffness element, as well as the axial displacement at the level of the reference axis for the 8DOF stiffness element. The solution iterative scheme is based on the secant method, with the convergence criteria relying on the ratios of the Euclidean norms of both forces and displacements. The advantage of the approach is that the displacement and force fields of the stiffness elements are extremely rich as they correspond to those required by the analytical solution of the elastic partial interaction problem, thereby producing a robust numerical technique. Experimental results available in the literature are used to validate the finite element proposed in the paper. For this purpose, those reported by Chapman and Balakrishnan (1964), Fabbrocino *et al.* (1998, 1999) and Ansourian (1981) are utilised; these consist of six simply supported beams with a point load applied at mid-span inducing positive bending moment in the beams, three simply supported beams with a point load applied at mid-span inducing negative bending moment in the beams, and six two-span continuous composite beams respectively. Based on these comparisons, a preferred degree of discretisation suitable for the proposed modelling technique expressed as a function of the ratio between the element length and depth is proposed, as is the number of Gauss stations needed. This allows for accurate prediction of the nonlinear response of composite beams.

Keywords : composite beams; nonlinear analysis; partial shear interaction; secant method; stiffness method.

1. Introduction

During the last century, many investigations were undertaken to understand and predict the behaviour of composite steel-concrete beams with partial shear interaction (PSI). In particular, the last decade or so has seen an increasing number of contributions investigating the behaviour of composite beams with PSI in the nonlinear range of material response being published. Newmark *et al.* (1951) demonstrated that full interaction theory was not always satisfactory in describing the behaviour of composite beams.

* Corresponding Author, Email: G.Ranzi@civil.usyd.edu.au

Many investigators have utilised or extended the work of this well-known paper and various nonlinear formulations have been produced. Nevertheless, it is beyond the scope of this paper to provide a lengthy discourse of the current state of the art, and useful reviews have been given by Pi *et al.* (2005a,b), Spacone and El-Tawil (2004), Leon and Viest (1996) and others. Because the problem is generally intractable to solutions in closed-form, numerical solutions must be used. Worthy of mention and relevant to the present study is the contribution by Faella *et al.* (2003), who extended the applicability of the 6DOF stiffness element previously derived (Faella *et al.* 2002) to account for the initial occurrence of material nonlinearities of the shear connection and concrete only. Their study intended to investigate the effects of the shear connection deformability on the service response of the beams and, for this purpose, they validated their approach against experiments published in the literature considering only low ranges of load.

At face value, popular commercial software packages such as Ansys (2003) and ABAQUS (2003) appear convenient for performing nonlinear analyses of composite beams, but some disquiet has been expressed regarding their accuracy and, in particular, their treatment of the shear connectors (Pi *et al.* 2005a). These packages can also suffer from being design tools, in which the underlying mechanics that describes the structural behaviour is often nebulous. Because of this, an alternative robust and accurate computational formulation has been sought in this paper.

The aim of the present study is to propose a novel modelling technique capable of depicting the behaviour of composite beams with PSI accounting for the material nonlinearity of all components of the cross-section. This is carried out by extending the applicability of two displacement-based elements, viz. a 6DOF stiffness element and an 8DOF one, that were derived by means of the direct stiffness method (DSM) and presented by the authors in the linear-elastic range of material response (Ranzi *et al.* 2004, Ranzi and Bradford 2007). The main advantage of the direct stiffness approach was that no interpolating approximations are introduced in the displacement and force fields. This work in the linear-elastic range highlighted the occurrence of numerical instabilities in the calculation of some stiffness coefficients for low values of the dimensionless stiffness parameter αL , that was identified by Girhammar and Pan (1993), when these coefficients are derived using exponential functions (or hyperbolic functions) in the expression for the slip, and it suggested a modelling procedure to avoid such instabilities.

The nonlinear solution strategy developed herein relies on an iterative scheme that utilises a secant procedure and whose convergence criteria is controlled by the ratios of Euclidean norms of both forces and displacements. The model validation is then carried out using experimental data available in the literature; the work by Chapman and Balakrishnan (1964), Fabbrocino *et al.* (1998, 1999) and Ansourian (1981) has been used here. In the validation stage, attention has been placed in ensuring that the material and cross-sectional properties of the beams analysed are as close as possible to those utilised and specified for the experiments (May *et al.* 2003), in order to provide more creditable comparisons of the computational scheme and experimental results.

2. Generic assumptions

The composite beam considered by the proposed direct stiffness formulation comprises of a concrete slab, steel reinforcement, a steel joist and shear connection as shown in Fig. 1. The top and bottom elements are referred to as elements 1 and 2 respectively. The composite cross-section $A \in \mathfrak{R}^2$ is represented more generically as $A = A_1 \cup A_2$, where A_1 and A_2 are the cross-sections of elements 1 and 2 respectively. The area A_1 represents the slab, and it is further sub-divided into areas A_c and A_r which are those of the concrete component and of the reinforcement respectively ($A_1 = A_c \cup A_r$), while A_2 represents the cross-

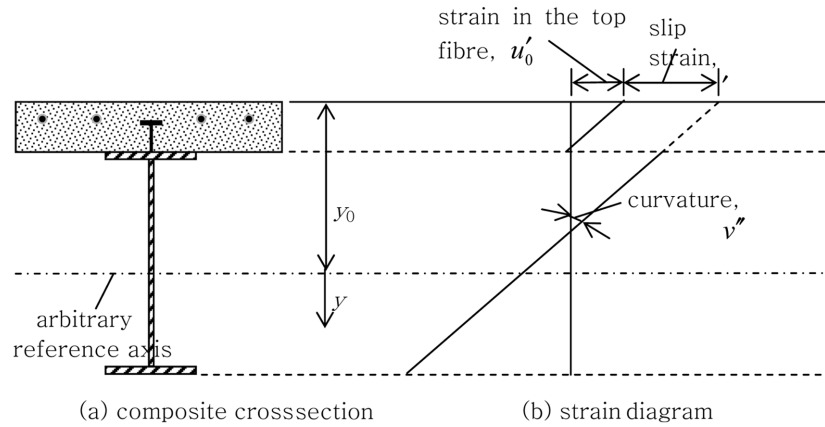


Fig. 1 Composite cross-section and strain diagram

section of the steel joist only and it is denoted as A_s . The strain diagram is defined uniquely by the strain in the top fibre of the cross-section u_0 , the curvature v'' and the slip strain s' , where the prime denotes a derivative with respect to the coordinate along the beam z . Implicit in this is the validity of the Euler-Bernoulli hypothesis that plane sections remain plane (except at the interface) and a linearization of the curvature for which v'^2 is deemed to vanish (Newmark *et al.* 1951). Similarly to Newmark's model, no vertical separation is assumed to occur between elements 1 and 2 (i.e. the top and bottom elements), so that the curvature is the same in both elements.

The composite beam is assumed to occupy the prismatic spatial region $V = A \times [0, L] \in \mathfrak{R}^3$, where A represents the composite cross-section which is assumed to be symmetric about the plane of bending, while $[0, L]$ is defined along the beam coordinate z (which is perpendicular to the cross-section at any location along the beam length, and with $z \in [0, L]$).

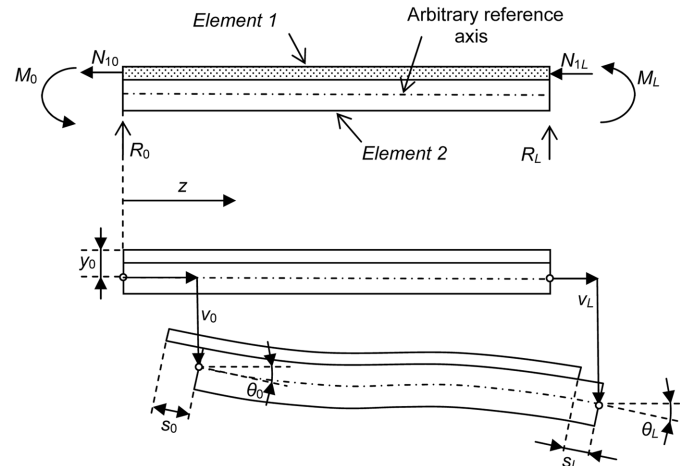
For generality, the model is derived with reference to an arbitrary axis located at a distance y_0 below the top fibre of the cross-section from which the cross-sectional properties of the beam are defined. As the axial displacement is controlled at the level of the reference axis, it will be assumed, without any loss of generality, that the reference axis is located in the steel joist (i.e. bottom element) as often occurs in real beams.

3. Nonlinear Modelling

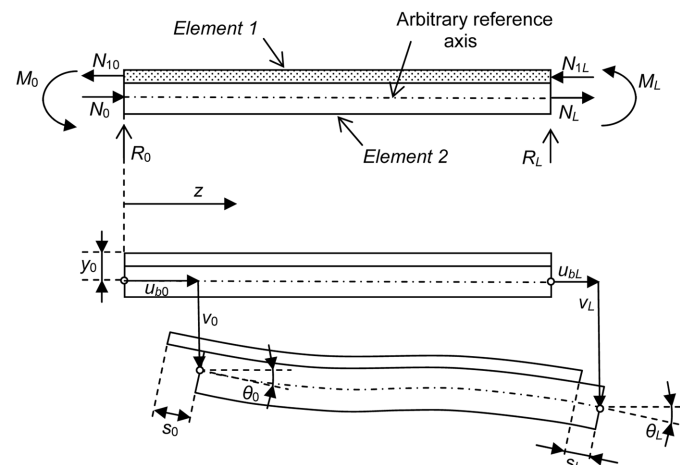
3.1. General

The applicability of two stiffness elements, i.e. the 6DOF and the 8DOF elements that were derived by means of the DSM in the linear-elastic range, is extended in this paper to account for material nonlinearities. The degrees of freedom of the 6DOF element are those related to the vertical displacement v , the rotation θ and the slip s , as shown in Fig 2(a). In the case of the 8DOF element the relevant freedoms include the vertical displacement v , the rotation θ , the slip s and the axial displacement u_b at the level of the arbitrary reference axis located y_0 below the top fibre of the cross-section as outlined in Fig. 2(b).

The secant stiffness method is utilised to perform the nonlinear analysis and, in this procedure, the load is incrementally and monotonically increased.



(b) Nodal displacements and actions of the 6DOF stiffness element



(a) Nodal displacements and actions of the 8DOF stiffness element

Fig. 2 Degrees of freedom of the 6DOF and 8DOF stiffness elements

3.2. General method of analysis

The analytical model utilised to derive both the 8DOF and 6DOF stiffness elements is constructed based on equilibrium considerations, and adopting a set of three independent parameters that are required to define the strain diagram; these unknowns are u_0' , v'' and s' .

For simplicity and again without loss of generality, a single span beam is considered subjected to a pattern of loading that produces a variation of the bending moment $M(z)$ and of the axial force $N(z)$ (referred to as M and N for simplicity), whose variations are not necessarily known initially if the beam is statically indeterminate.

The governing system of equations can be written by enforcing horizontal and rotational equilibrium at the composite cross-section, as well as horizontal equilibrium of a free body diagram of the top element (Fig. 3) as

$$N_i = \int_A \sigma dA = N \quad ; \quad M_i = \int_A y\sigma dA = M \quad ; \quad N_1' + q = 0 \quad (1a,b,c)$$

where N_i and M_i are the internal axial force and moment resisted by the composite cross-section, σ is the generic stress in the composite cross-section, N_1 is the axial force resisted by the top element, and q represents the force per unit length resisted by the shear connection.

Based on Eqs. (1) and after some mathematical manipulation, the governing differential equation can be obtained as (Ranzi *et al.* 2003)

$$\tilde{\alpha}s'' - ks = \alpha M' + \alpha_1 N', \quad (2)$$

where s is the slip along the member length, all cross-sectional variables are defined in the appendix. The homogeneous and the particular solutions of the PSI problem in Eq. (2), s_H and s_P respectively, can then be written in compact form as

$$s = s_H(C_1, C_2) + s_P \quad (3a)$$

$$s' = s'_H(C_1, C_2) + s'_P \quad (3b)$$

in which

$$s_H = C_1 e^{\mu z} + C_2 e^{-\mu z} \quad (4a)$$

$$s'_H = \mu C_1 e^{\mu z} - \mu C_2 e^{-\mu z}, \quad (4b)$$

and where the actual expression for s_P depends on the loading and support conditions of the problem, and in which C_1 and C_2 are constants of integration.

The other two unknown variables, i.e. u'_0 and v'' , can then be determined as

$$u'_0 = b_1 M + b_2 N + b_3 s' \quad (5a)$$

$$v'' = r_1 M + r_2 N + r_3 s', \quad (5b)$$

where all the notation is defined in the appendix. Finally, the full set of variables depicting the displacement field can be determined by integrating the parameters describing the strain diagram. In this process, the

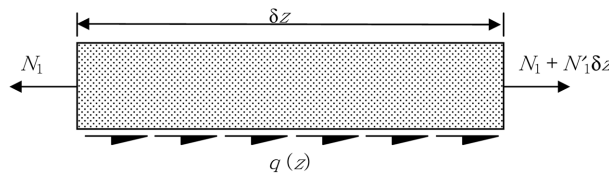


Fig. 3 Free body diagram of the top element

constants of integration can be determined utilising the appropriate static and/or kinematic boundary conditions of the problem under consideration (Ranzi *et al.* 2004, Ranzi and Bradford 2007). Denoting the generic stress in element 1 as σ_1 , the axial force resisted by element 1 (i.e. the reinforced concrete slab), which is also needed for the direct stiffness technique, is calculated as

$$N_1 = \int_{A_1} \sigma_1 dA = q_1 M + q_2 N + q_3 s' \quad (6)$$

where all notation is defined in the appendix.

3.3. Derivation of the 6DOF and 8DOF stiffness elements

The derivation of the 6DOF and 8DOF stiffness elements has already been presented in the linear-elastic range and, with full detail being given by Ranzi *et al.* (2004) and Ranzi and Bradford (2007) respectively. The stiffness coefficients are derived herein by means of the DSM utilising the modelling procedure outlined in Eqs. (2) to (6) (Weaver and Gere 1990).

The main difference regarding the loading conditions considered by the 8DOF and the 6DOF formulations is that in the latter one no axial force can be resisted by the composite cross-section while in the former one the composite cross-section is able to resist axial loading. This difference is introduced when enforcing horizontal equilibrium in the formulation utilised for the DSM. In the case of the 6DOF element the sum of the horizontal forces resisted by the slab and steel joist is equated to zero. This limitation is released for the 8DOF element in which case the expression for horizontal equilibrium includes a term representing the external applied axial force.

The system of equations to be solved based on the DSM method can then be expressed as:

$$\vec{q}_m + \vec{q}_{eq,m} = \begin{bmatrix} k_{11} & k_{12} & \dots & k_{1m} \\ & k_{22} & & \\ & & \ddots & \\ & & & k_{mm} \end{bmatrix} \vec{d}_m = \bar{K}_m \vec{d}_m \quad (7)$$

in which $m = 6$ and 8 for the 6DOF and 8DOF stiffness elements respectively, and

$$\vec{q}_6 = [R_0, M_0, N_{10}, R_L, M_L, N_{1L}]^T \quad (8a)$$

$$\vec{q}_8 = [N_0, R_0, M_0, N_{10}, N_L, R_L, M_L, N_{1L}]^T \quad (8b)$$

$$\vec{d}_6 = [v_0, v'_0, s_0, v_L, v'_L, s_L]^T \quad (8c)$$

$$\vec{d}_8 = [u_{n0}, v_0, v'_0, s_0, u_{nL}, v_L, v'_L, s_L]^T \quad (8d)$$

where \vec{q}_m and \vec{d}_m are the vectors of nodal actions and displacements shown in Fig. 2, $\vec{q}_{eq,m}$ is the

vector of equivalent nodal loads due to member loads, k_{ij} are the stiffness coefficients ($i = 1, \dots, m$; $j = 1, \dots, m$), and \bar{K}_m is the appropriate element stiffness matrix. In this definition, the slip may be thought of as being conjugate in an abstract sense to the axial force within element 1.

Based on the DSM method, the j -th column of the stiffness matrix equals the set of unknown reactions determined for an unloaded member whose freedoms are all restrained except for the one related to the j -th column, for which a unit displacement is imposed. The secant coefficients included in the matrices \bar{K}_m for both 6DOF and 8DOF elements are similar to those obtained in the linear-elastic range by Ranzi *et al.* (2004) and Ranzi and Bradford (2007), but by modifying the elastic properties, i.e. moduli and shear connection stiffnesses, with their appropriate secant values.

Small monotonic increments are specified in this study to trace the loading path of the beams adequately. For each load step, different iterations have been performed to converge to the final solution, as is well-documented in textbooks on nonlinear analysis (Reddy 2004). A layered model has been adopted as the basis of the proposed nonlinear procedure to represent the composite cross-sectional properties (Reddy 2004, Zhang *et al.* 2006), which subdivides the composite cross-section into layers perpendicular to its axis of symmetry. Reinforcing bars located at the same level from the reference axis are placed in the same layer, whose centroid is located at the centroids of the reinforcing bars, while the concrete slab is layered ignoring the areas filled by the reinforcement. The steel joist is modelled layering both the flanges and the web. Material states at each layer are evaluated at their mid-height based on the nonlinear constitutive law of the material under consideration. To evaluate the material state of an element, one or more cross-sections can be considered along the element itself; these are located at the Gauss stations commonly used for lengthwise integration by means of the Gauss-Legendre quadrature.

Based on the previous considerations, the secant composite cross-sectional properties and secant shear connection properties to be used for each stiffness element m in Eq. (7) at the i -th iteration of the l -th load step are determined as:

$$A\tilde{E}_{S1.m.li} = \sum_{g=1}^{g_{\max}} w_g \sum_{j=1}^{j_{\max1}} A_{m.gj} E_{m.ligj} ; \quad A\tilde{E}_{S2.m.li} = \sum_{g=1}^{g_{\max}} w_g \sum_{j=j_{\max1}+1}^{j_{\max2}} A_{m.gj} E_{m.ligj} \quad (9a,b)$$

$$B\tilde{E}_{S1.m.li} = \sum_{g=1}^{g_{\max}} w_g \sum_{j=1}^{j_{\max1}} y_{m.gj} A_{m.gj} E_{m.ligj} ; \quad B\tilde{E}_{S2.m.li} = \sum_{g=1}^{g_{\max}} w_g \sum_{j=j_{\max1}+1}^{j_{\max2}} y_{m.gj} A_{m.gj} E_{m.ligj} \quad (9c,d)$$

$$I\tilde{E}_{S1.m.li} = \sum_{g=1}^{g_{\max}} w_g \sum_{j=1}^{j_{\max1}} y_{m.gj}^2 A_{m.gj} E_{m.ligj} ; \quad I\tilde{E}_{S2.m.li} = \sum_{g=1}^{g_{\max}} w_g \sum_{j=j_{\max1}+1}^{j_{\max2}} y_{m.gj}^2 A_{m.gj} E_{m.ligj} \quad (9e,f)$$

$$A\tilde{E}_{S.m.li} = A\tilde{E}_{S1.m.li} + A\tilde{E}_{S2.m.li} ; \quad B\tilde{E}_{S.m.li} = B\tilde{E}_{S1.m.li} + B\tilde{E}_{S2.m.li} \quad (9g,h)$$

$$I\tilde{E}_{S.m.li} = I\tilde{E}_{S1.m.li} + I\tilde{E}_{S2.m.li} ; \quad k_{S.m.li} = \sum_{g=1}^{g_{\max}} w_g k_{S.m.lig} \quad (9i,j)$$

where g is the Gauss station considered along member m , j identifies the layer of the cross-section, the top element (i.e. reinforced concrete slab) is assumed to be subdivided into $j_{\max1}$ layers with $j = 1$,

... j_{max1} , the composite cross-section is subdivided into j_{max2} layers while the bottom element (i.e. steel joist) is subdivided into $j_{max2} - j_{max1}$ layers with $j = j_{max1} + 1, \dots, j_{max2}$, g_{max} is the number of Gauss stations considered in the stiffness element, w_g is the Gauss weight at the g -th Gauss station, $A_{m,gj}$ is the area of the j -th layer at the g -th Gauss station of member m , $E_{m,ligj}$ is the secant modulus of the material located at the j -th layer at the g -th Gauss station of member m at the i -th iteration of the l -th load step, $y_{m,gj}$ is the distance between the reference axis and the centroid of the j -th layer at the g -th Gauss station of member m , $k_{S,m,lig}$ is the secant shear connection stiffness determined based on the shear flow and slip calculated at the location of the g -th Gauss station of member m at the i -th iteration of the l -th load step, $k_{S,m,li}$ is the secant shear connection stiffness of member m at the i -th iteration of the l -th load step, and $\tilde{A}E_{S1,m,li}$, $\tilde{B}E_{S1,m,li}$, $\tilde{I}E_{S1,m,li}$, $\tilde{A}E_{S2,m,li}$, $\tilde{B}E_{S2,m,li}$, $\tilde{I}E_{S2,m,li}$, $\tilde{A}E_{S,m,li}$, $\tilde{B}E_{S,m,li}$, $\tilde{I}E_{S,m,li}$ are the secant cross-sectional properties calculated at the i -th iteration of the l -th load step of member m .

3.4. Numerical instabilities

The use of the stiffness relationship expressed by Eq. (7) can lead to numerical instabilities in the calculation of the stiffness coefficients for both the 6DOF and 8DOF elements at low values of the dimensionless shear connection stiffness μL , which is defined in appendix and is equivalent to the dimensionless stiffness αL introduced by Girhammar and Pan (1993) and where L is the element length. This problem has already been identified by the authors and originates from the lack of numerical precision introduced by the large terms which arise when the exponentials in μL are inverted within the stiffness relationships and are multiplied with other exponentials in μL , leading to a loss of significant figures in the calculated number stored by the computer. These exponential functions appear in the solution of the governing differential equation in Eqs. (3) and (4). It was noted that this undesirable behaviour occurred only for very low values of μL , i.e. for $\mu L < 0.05$ as quantitatively depicted in Fig. 4. In these cases the solution for the slip in Eqs. (3) and (4) has been modified by replacing the exponentials in Eq. (4) with their Taylor series expansion truncated at the eighth term as

$$s = C_1 \sum_{j=0}^7 \frac{(\mu z)^j}{j!} + C_2 \sum_{j=0}^7 (-1)^j \frac{(\mu z)^j}{j!} + s_p. \quad (10)$$

By using this technique, the proposed modelling procedure relies on two stiffness matrices; one derived expressing the slip with exponential functions (Eq. (4)) and one with their truncated Taylor series expansion (Eq. (10)). Therefore, the stiffness coefficients calculated for an element whose dimensionless stiffness coefficient μL is greater than 0.05 are based on the exponential expression for the slip, while for μL less than 0.05 these are based on their truncated Taylor expansion. The dimensionless stiffness μL is not just dependent upon the structural system considered, but also upon the discretisation utilised as L represents the length of the stiffness element. This instability needs to be addressed in the nonlinear modelling since low values of μL calculated for a certain element can be achieved due to a fine discretisation of the beam analysed, or due to the material nonlinearities which affect the secant cross-sectional properties included in μL . The robustness of the modelling technique is guaranteed by verifying that the two stiffness matrices, i.e. those based on the exponentials and its counterpart based on the truncated Taylor series, can be interchanged. This is carried out ensuring that the coefficients of both stiffness matrices are identical for μL equal to 0.05 regardless of the actual value of μL for the element.

In general, a robust numerical model to be used to describe the nonlinear behaviour of composite

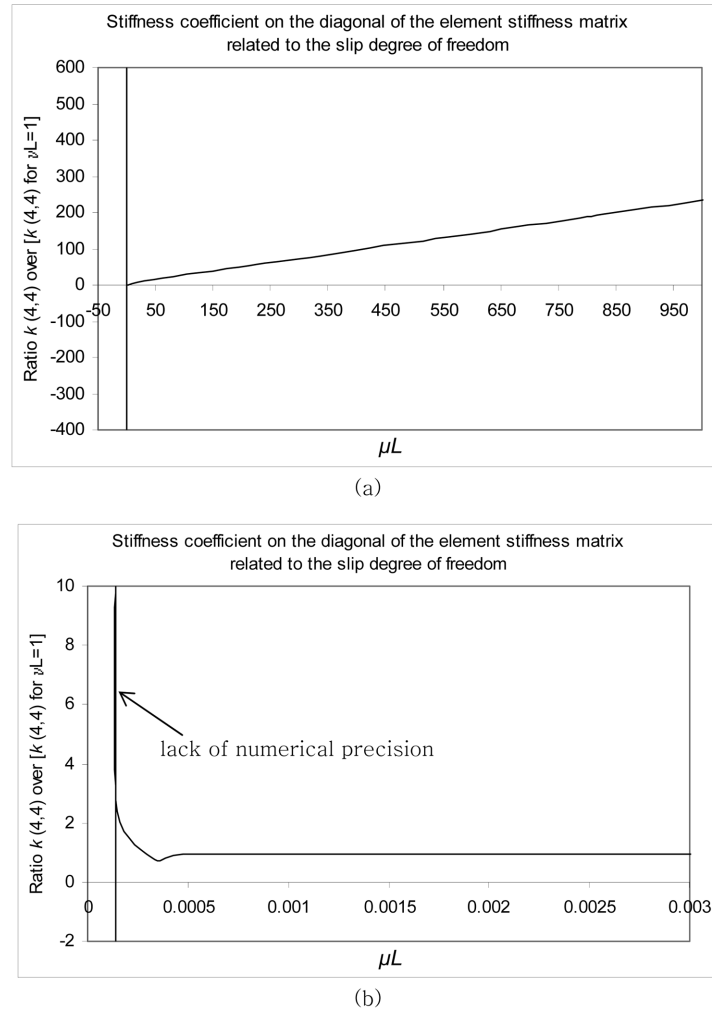


Fig. 4 Numerical instabilities of the stiffness coefficient related to the slip using the exponential approach for varying μL

members requires to easily handle both situations of high and low stiffness values also reflected by high and small values for μL calculated at the element level. This is particular important as the nonlinear behaviour of the shear connection can lead to secant stiffness values ranging from extremely high ones at locations of negligible slip, for example at an internal support of a two-span continuous beam, to very small ones exhibited when large relative movements between the slab and steel joist have taken place, usually occurring at the end supports of a beam system.

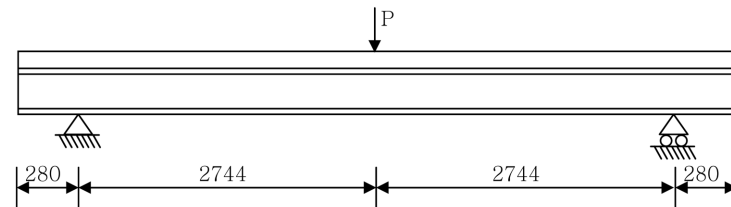
Finally, the solution convergence criterion utilised in the solution strategy of the nonlinear computational model is based on the ratios of the Euclidean norms of both displacements and forces. The ratio of the Euclidean norms of the forces has been utilised to ensure the stability of the iterative scheme as, in the case of a uniformly distributed load, the equivalent nodal loads placed in the loading vector conjugate to the slip degrees of freedom are expressed in terms of the cross-sectional properties of the element.

4. Validations

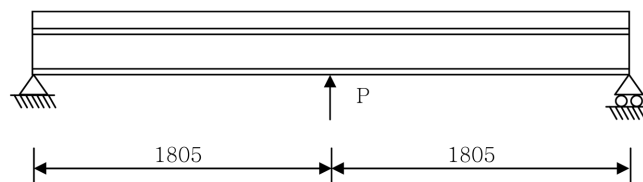
4.1. General

The nonlinear modelling technique presented is validated in this section against experimental results available in literature. For this purpose, the following three benchmark experiments have been considered.

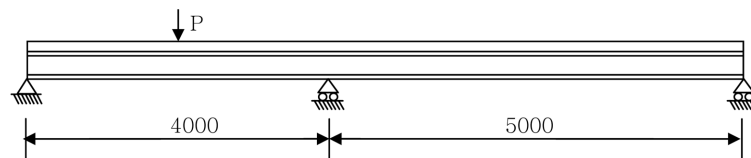
- Six simply supported beams subjected to a point load applied at mid-span tested by Chapman and Balakrishnan (1964). (Beams A1, A2, A3, A4, A5 and A6). Their layouts are shown in Fig. 5(a) and their cross-sectional and material properties are summarised in Table 1.
- Three simply supported beams subjected to a point load applied at mid-span, which induces negative bending moment in the beam, reported by Fabbrocino *et al.* (1998, 1999). (Beams A, B and C.) Their layouts are shown in Fig 5(b) and their cross-sectional and material properties are summarised in Table 2.



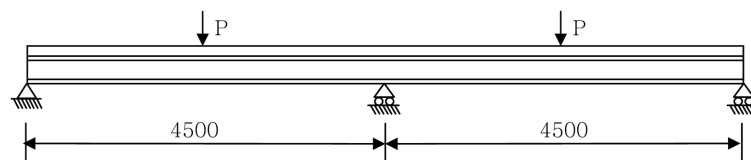
Beams tested are referred to as: A1, A2, A3, A4, A5, A6
(a) Experiments reported by Chapman and Balakrishnan (1964)



Beams were tested in negative bending and are referred to as: A, B, C
(b) Experiments reported by Fabbrocino *et al.* (1998, 1999)



Beams are referred to as: CTB1 and CTB2



Beams are referred to as: CTB3, CTB4, CTB5 and CTB6
(c) Experiments reported by Ansourian (1981)

Fig. 5 Layout, support and loading conditions of the beams used in the validation process

Table 1 Cross-sectional and material properties of the beam tests reported in (Chapman and Balakrishnan 1964)

	Beams					
	A1	A2	A3	A4	A5	A6
Depth of composite cross-section (mm)	457.2	457.2	457.2	457.2	457.2	457.2
Slab width (mm)	1219.2	1219.2	1219.2	1219.2	1219.2	1219.2
Slab depth (mm)	152.4	152.4	152.4	152.4	152.4	152.4
Concrete cylinder strength (MPa)	22.1	26.9	18.3	20.1	24.8	23.7
No of connectors	84	76	68	56	44	32
Spacing in pairs of connectors (mm)	144.8	158.8	177.8	215.9	274.3	378
Ultimate capacity of single studs (kN)	Mean value of 121.4 (max of 127 and min of 113)					
Steel joist	12" × 6" × 44 lb B.S.B.					
Young's modulus - flange of joist (MPa)	179263	184779	176505	176505	177884	191674
Young's modulus - web of joist (MPa)	187537	183400	182021	186158	184779	184779
Yield stress - flange of joist (MPa)	215	217	274	276	263	239
Yield stress - web of joist (MPa)	208	208	229	229	210	214
Ultimate stress - flange of joist (MPa)	371	379	403	396	403	416
Ultimate stress - web of joist(MPa)	368	372	405	396	403	378
Ratio of strain at strain-hardening over yield strain - flange of joist	12.4	7.6	1	1	1	1.5
Ratio of strain at strain-hardening over yield strain -web of joist	9.6	4.9	1	1.8	1	1.7
* Yield strain - flange of joist	1200e ⁻⁶	1175e ⁻⁶	1555e ⁻⁶	1563e ⁻⁶	1481e ⁻⁶	1247e ⁻⁶
* Yield strain – web of joist	1108e ⁻⁶	1135e ⁻⁶	1257e ⁻⁶	1232e ⁻⁶	1138e ⁻⁶	1160e ⁻⁶
* Strain at strain-hardening – flange of joist	1488e ⁻⁵	893e ⁻⁵	155e ⁻⁵	156e ⁻⁵	148e ⁻⁵	187e ⁻⁵
* Strain at strain-hardening – web of joist	1064e ⁻⁵	556e ⁻⁵	126e ⁻⁵	222e ⁻⁵	114e ⁻⁵	197e ⁻⁵
* Ultimate strain – flange of joist	5439e ⁻⁵	4879e ⁻⁵	3458e ⁻⁵	3245e ⁻⁵	3706e ⁻⁵	4395e ⁻⁵
* Ultimate strain – web of joist	4950e ⁻⁵	4623e ⁻⁵	4536e ⁻⁵	4285e ⁻⁵	4845e ⁻⁵	4217e ⁻⁵
** Strain-hardening modulus – flange of joist (MPa)	3944	4065	3883	3883	3913	4217
** Stain-hardening modulus – web of joist (MPa)	4126	4035	4004	4095	4065	4065
Longitudinal reinforcement, mm ²						
Top layer	200	200	200	200	200	200
Bottom layer	200	200	200	200	200	200

* values have been calculated based on a trilinear constitutive model for the steel material

** a ratio of slope of strain-hardening line to Young's modulus of 0.022 is assumed as adopted in the modelling presented in (Yam and Chapman 1968)

· Six continuous two-span beams tested by Ansourian (1981). Two beams (CTB1 and CTB2) were loaded by a point load applied at the centre of the left span while the right span remained unloaded; four beams (CTB3, CTB4, CTB5 and CTB6) were loaded by point loads applied at the centres of both spans. Their layouts are shown in Fig. 5(c) and their cross-sectional and material properties are summarised in Tables 2 and 4 respectively.

4.2. Validation process

Three main issues have been investigated in modelling the experiments with the DSM: (i) the number

Table 2 Cross-sectional and material properties of the beam tests reported in (Fabbrocino *et al.* 1998, 1999)

	Beams		
	A	B	C
Steel joist	HEB180	HEB180	HEB180
Depth of the composite cross-section (mm)	300	300	300
Slab width (mm)	800	800	800
Slab depth (mm)	120	120	120
Concrete cubic strength (MPa)	30	30	30
Steel reinforcement	4 off 14 mm (dia.) bars	4 off 14 mm (dia.) bars	4 off 14 mm (dia.) bars
Shear connectors	16 mm dia. 100 mm high	16 mm dia. 100 mm high	16 mm dia. 100 mm high

NOTE: material properties for the steel joist and the steel reinforcement have been obtained from the experimental stress-strain relationships reported in (Fabbrocino *et al.* 1999)

Table 3 Cross-sectional properties of the beam tests reported in (Ansourian 1981)

		Beams					
		CTB1	CTB2	CTB3	CTB4	CTB5	CTB6
Spans, m		4 × 5	4 × 5	4.5 × 4.5	4.5 × 4.5	4.5 × 4.5	4.5 × 4.5
Jack loading		Centre of left span	Centre of left span	Centre of each span	Centre of each span	Centre of each span	Centre of each span
Slab	Thickness, mm	100	100	100	100	100	100
	Width, mm	800	1300	1300	800	1300	1300
Joist	Section	IPE 200 × 22.4 kg	IPE 200 × 22.4 kg	IPBL 200 × 22.4 kg	IPE 200 × 22.4 kg	IPE 200 × 22.4 kg	IPE 200 × 22.4 kg
	Area, mm ²	2850	2850	5380	5380	3910	3910
	Flange, mm	8.5 × 100	8.5 × 100	10 × 200	10 × 200	9.8 × 100	9.8 × 120
	Web, mm	5.6	5.6	6.5	6.5	6.2	6.2
Number of 19 mm × 75 mm Nelson studs		66	66	84	84	60	60
Percentage shear connection	Sagging	150	150	160	150	120	110
	Hogging	160	135	130	130	105	95
Longitudinal reinforcement, mm ²	Hog top	800	1230	1230	804	1260	1260
	Hog bottom	316	470	470	767	470	767
	Sag top	-	360	360	160	320	380
	Sag bottom	160	160	160	160	160	160
Transverse reinforcement		10 mm diameter at 100 mm at bottom of slab					

of layers adopted for the cross-section, (ii) the degree of discretisation required to obtain an adequate description of the experiments, expressed as a function of the ratio ψ_{LD} of the element length to its depth, and (iii) the minimum number of Gauss stations required by the preferred degree of discretisation to produce acceptable results. The number of Gauss stations is important in the calculation of the secant cross-sectional and material properties in Eqs. (9) and the interplay of these with the discretisation in a layered modelling has been shown to be significant (Sun *et al.* 1994).

A simple procedure is proposed here to determine the minimum number of layers that need to be

Table 4 Material properties of the beam tests reported in (Ansourian 1981)

		Beams					
		CTB1	CTB2	CTB3	CTB4	CTB5	CTB6
200 mm cube strength, N/mm ²		30	50	43	34	29	41
Density of concrete, kg/m ³		2310	2310	2350	2280	2300	2300
Lower yield stress, N/mm ²	Flange	277	277	220	236	265	292
	Web	340	340	235	238	278	310
	Reinforcement	430	430	430	430	430	430
Ultimate tensile stress, N/mm ²	Flange	421	418	390	393	442	462
	Web	440	477	411	401	428	450
	Reinforcement	533	533	533	533	533	533
Strain at strain-hardening, ϵ_{sh}		0.012	0.018	0.017	0.018	0.019	0.014
Initial strain-hardening modulus E_{sh} , N/mm ²		6000	4200	5000	3000	4800	3800

specified in the analysis. Using elastic material properties, this procedure requires that the flexural rigidity determined numerically with layering is within 0.01% of that determined analytically without layering, since the flexural rigidity of a layer about its own centroid is ignored in the computational scheme. For the three experimental series considered, the number of layers needed varied between 40 and 70.

No simple procedure can be utilised to determine the preferred degree of discretisation when using the proposed DSM elements, i.e. preferred values for ψ_{LD} , and the minimum number of Gauss stations required by these preferred options. This was also concluded in the nonlinear layered finite element analysis of reinforced concrete beams by Sun *et al.* (1993). For this reason, the model validation was carried out varying the number of elements as outlined in Table 5, i.e. varying the degree of discretisation as a function of ψ_{LD} , and the number of Gauss stations utilised in the solution strategy. The number of elements has been varied from the minimum number needed to model the applied loading and the cross-sectional properties to a maximum number of elements (of equal length) whose element coefficient ψ_{LD} is approximately equal to 0.5. For each discretisation, the number of Gauss stations was varied between 3 and 24.

The aim of the model validation is to establish whether or not the proposed nonlinear modelling technique presented can adequately predict the structural behaviour of composite beams with PSI accounting for material nonlinearities and, if this is the case, to determine the preferred values for the element coefficient ψ_{LD} for its use and the associated minimum number of Gauss stations. This is carried out in two stages.

For Stage 1, graphical comparisons are carried out between the numerical results utilising predetermined discretisations in order to determine which degrees of discretisation (defined in terms of ψ_{LD}) adequately describe the experimental behaviour; the discretisations relevant to the validations herein are given in Table 5. Stage 2 compares the numerical solutions for each adopted discretisation relative to those obtained using 24 Gauss stations. For this study, 3, 5, 7, 12 and 24 Gauss stations were utilised, and the solution using ng Gauss stations was deemed to be acceptable when the error relative to that with $ng = 24$ Gauss stations was less than a predetermined difference η . This strategy requires the load

$$P = \min[P_{max, ng}, P_{max, 24}] \tag{11}$$

Table 5 Discretisations adopted in the modelling of the experiments

Experiments reported in (Chapman and Balakrishnan 1964)				
No. of elements (Beams A1, A2, A3, A4, A5 and A6)	4	8	14	26
$\psi_{L/D}$	varies*	≈ 2	≈ 1	≈ 0.5
Experiments reported in (Fabbrocino <i>et al.</i> 1998, 1999)				
No. of elements (Beams A, B and C)	2	6	12	24
$\psi_{L/D}$	≈ 6	≈ 2	≈ 1	≈ 0.5
Experiments reported in (Ansourian 1981)				
No. of elements (Beams CTB1 and CTB2)	5	15	30	60
$\psi_{L/D}$	varies*	≈ 2	≈ 1	≈ 0.5
No. of elements (Beams CTB3 and CTB4)	6	18	32	64
$\psi_{L/D}$	varies*	≈ 2	≈ 1	≈ 0.5
No. of elements (Beams CTB5 and CTB6)	6	16	28	56
$\psi_{L/D}$	varies*	≈ 2	≈ 1	≈ 0.5

* for the coarsest possible discretisation, the element coefficient $\psi_{L/D}$ varies along the beam length as the discretisation considered is based on the minimum number of elements and, therefore, the element lengths might vary as governed by the layout, cross-sectional properties, loading and support conditions of the beam considered

to be determined, where $P_{\max,ng}$ and $P_{\max,24}$ are the maximum or peak loads obtained in the numerical analysis with ng and 24 Gauss stations respectively, and the relative error $e_{ng}(X)$ for a variable X (representing a displacement, strain, stress or the like) to be determined from

$$e_{ng}(X) = [X_{ng}(P) - X_{24}(P)] / X_{24}(P). \quad (12)$$

For a particular variable X , the error is acceptable when $e_{ng}(X) \leq \eta$, with η being somewhat arbitrarily taken here as 1%. It is worth noting that in the analyses carried out as part of the proposed study it has been observed that the number of Gauss stations specified in the solution process heavily affects the computational time of the analysis and, therefore, needs to be kept to a minimum. Varying the number of elements utilized in the mesh also affected the overall analysis time even if to a smaller extent.

It is worth noting that the results obtained in the modelling of the experiments by means of the 6DOF and 8DOF stiffness elements are identical as no axial force is induced along the beams considered. This is possible as in all experiments considered there is no external horizontal restraint provided to the tested beams.

4.3. Experiments by Chapman and Balakrishnan (1964)

Chapman and Balakrishnan (1964) reported material properties that are summarised partly in Table 1, and this data was used to model the concrete using the CEB-FIB guidelines (1993) as highlighted in Fig. 6, whilst the reinforcing steel and joist were modelled using the trilinear representation of Fig. 7. It is worth noting that the ratios of the strain at the onset of strain hardening to the yield strain varied significantly for the beams (being as low as 1 for the flanges of beams A3, A4 and A5), and so Yam and Chapman (1968) also used a trilinear representation of the stress-strain relationship to model these experiments.

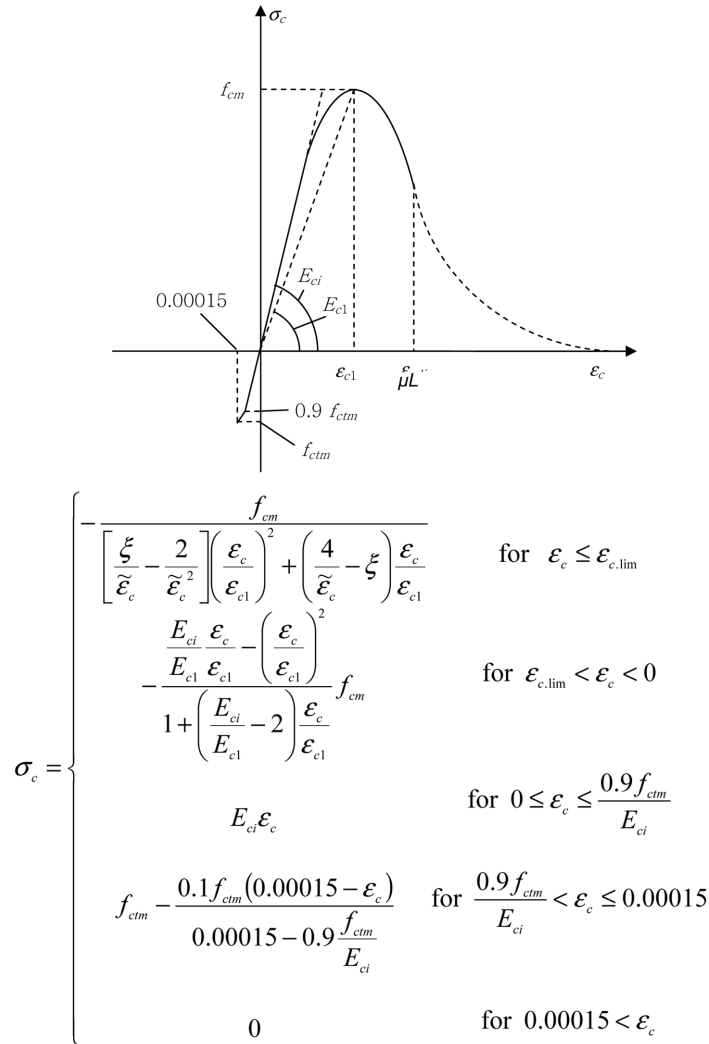


Fig. 6 Nonlinear constitutive law for the concrete material (CEB-FIB 1993)

The shear connection was modelled as described in Fig. 8, adopting the values $\alpha = 0.74$ and $\beta = 1.22$, based on the push-out test data, while the experimental values for the yield strains, strains at the onset of strain hardening and strains at ultimate stress reported by Chapman and Balakrishnan (1964) were used in the numerical modelling. The strain-hardening modular ratio E_{sh}/E_s (Fig. 8) was taken to be 1/45, as was also assumed by Yam and Chapman (1968).

It is noteworthy that the deflection curves presented by Chapman and Balakrishnan (1964) seem to contain an inconsistency: two different deflection curves have been referenced for the same beam (beam A4). For the purpose of this study, the higher of the two curves has been utilised to compare the deflection results for beam A4. Due to the same inconsistency, the second of these curves has been considered in the comparison for the deflections of beam A5; this has been carried out on the basis that this curve would provide more consistent results with the moment-curvature curve of beam A5 than the deflection curve labelled with A5 of Chapman and Balakrishnan (1964).

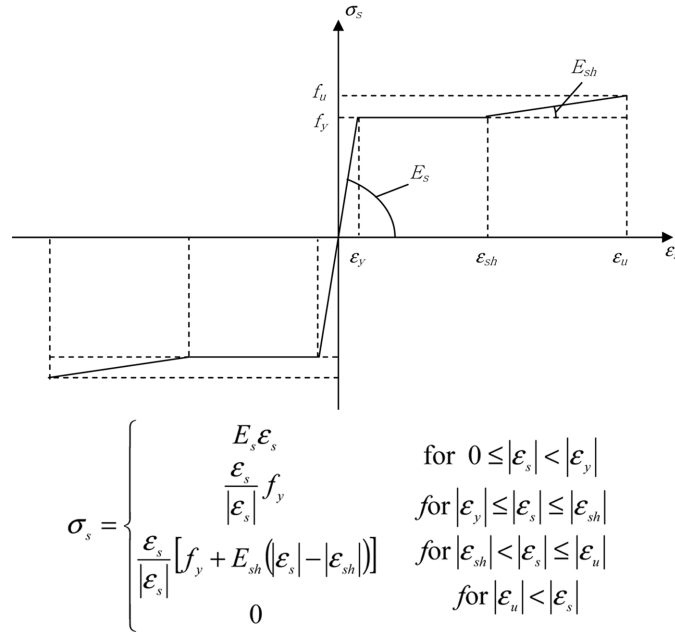


Fig. 7 Nonlinear constitutive law for the steel: trilinear model

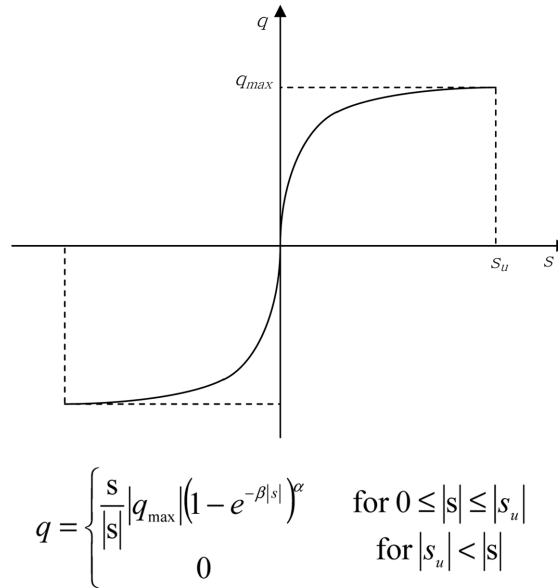


Fig. 8 Nonlinear constitutive law for the shear connection

The graphical comparison (Stage 1) for these beams is illustrated in Figs. 9 and 10, which show the mid-span deflections and curvatures for beams A1~A4 (Fig. 9) and A5 and A6 (Fig. 10). In general, the discretisations based on 14 and 26 elements (Table 5) predict both the load-deflection and the moment-

curvature curves of the tests quite well, although sometimes the former discretisation overestimates the beam stiffness and capacities. The results obtained using the 4 and 8 element meshes did not describe the structural response of the beams adequately.

The deflections and the curvatures at mid-span have also been considered in the comparisons of results

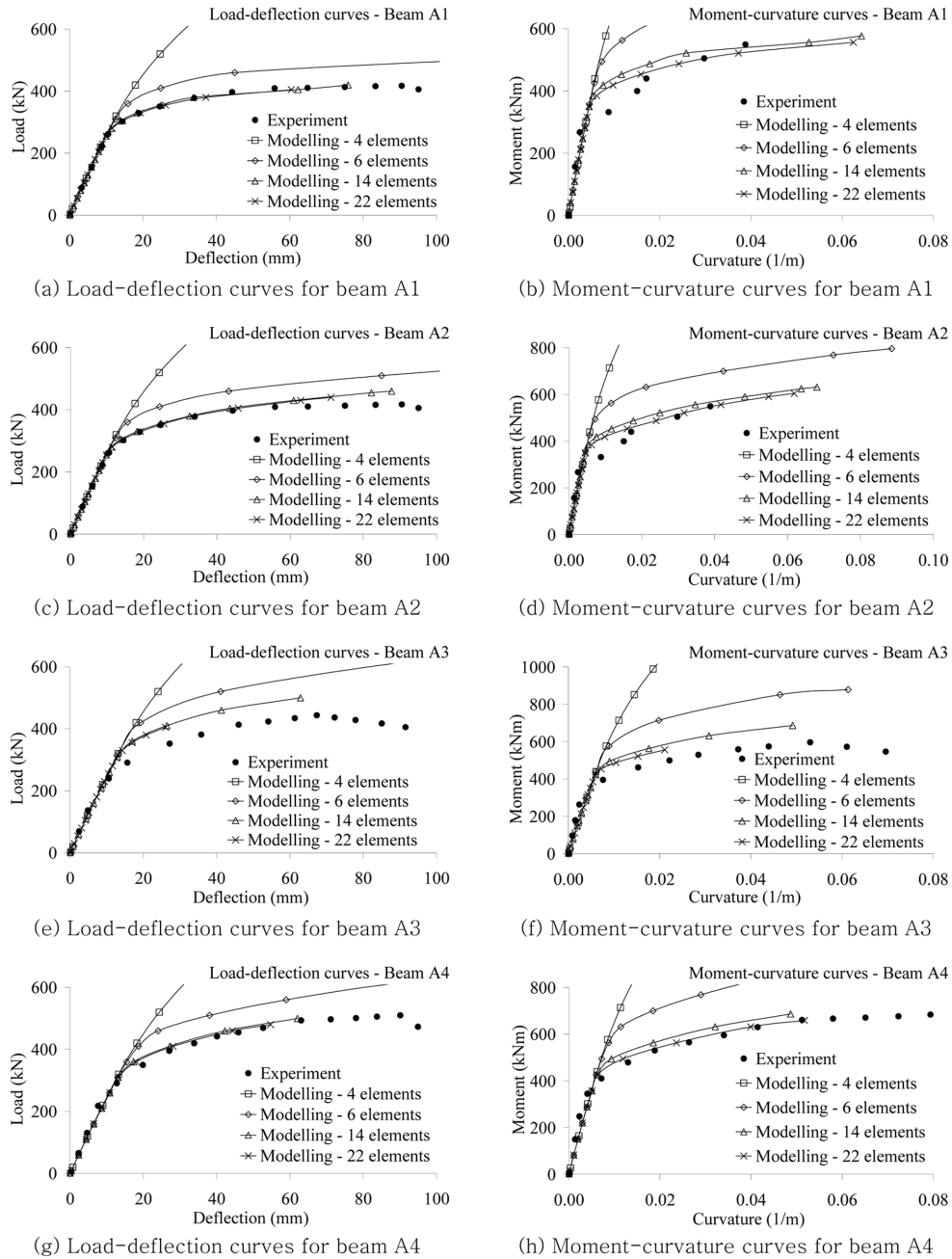


Fig. 9 Experimental results for beams A1 and A4 (Chapman and Balakrishnan 1964)

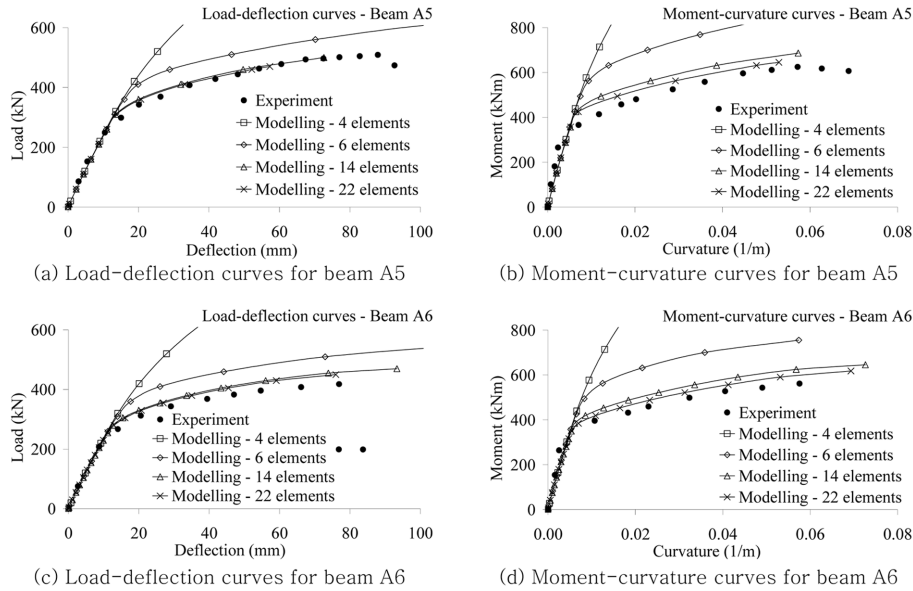


Fig. 10 Experimental results for beams A5 and A6 (Chapman and Balakrishnan 1964)

for different numbers of Gauss stations (Stage 2). Table 6 shows the results for the coarser discretisations (higher values of $\psi_{L/D}$) for 3, 5, 7 and 12 Gauss stations needed to keep the error e_{ng} relative to that for 24 Gauss stations below $\eta = 1\%$, when based on the same discretisation. From the results of all numerical simulations, 3 Gauss stations were found to be sufficient with 14 and 26 elements, except for beams A3 and A6 which needed a larger number of elements to keep $e_{ng} < 1\%$. Beams meshed with 4 or 8 elements required 5 or more Gauss stations.

4.4. Experiments by Fabbrocino *et al.* (1998, 1999)

The experiments reported by Fabbrocino *et al.* (1998, 1999) have been used to model the material properties for the numerical simulations of beams A, B and C. For these, the CEB-FIB guidelines (1993) have been used for the concrete slab (Fig. 6). For these kinds of problems it is very important to select an appropriate constitutive model for the tensile behaviour of the concrete in order to be able to well depict not only the generalised displacements of the problem but also its deformation state, i.e. strains and curvature. The quadrilinear representation of Fig. 11 was used for the steel joist and reinforcement as it better represents the experimental stress-strain curves reported by Fabbrocino *et al.* (1998, 1999). The representation of the shear connection in Fig. 8 was used with $\alpha = 0.3$ and $\beta = 0.3$ to match the push test results reported by Fabbrocino *et al.* (1999).

The graphical comparisons (Stage 1) carried out for beams A, B and C considered several variables as shown in Figs. 12 and 13. These variables are the deflection at mid-span, the curvature measured 210 mm from mid-span, the slip at the beam ends and the compressive and tensile strains in the top and bottom fibres of the steel joist measured 210 mm from mid-span for beams A and B. For beam C, the variables considered were the deflection at mid-span, the curvature measured 140 mm from mid-span, the slip at the beam ends and the compressive and tensile strains in the top and bottom fibres of the steel joist measured 680 mm and 140 mm from mid-span respectively.

Table 6 Nonlinear modelling results for beams reported in (Chapman and Balakrishnan 1964)

BEAM	Variable	P = peak load of the analysis in kN A = deflection at mid-span in mm at peak load [error %] B = curvature in 1/m at peak load [error %]			
		3 Gauss stations	5 Gauss stations	7 Gauss stations	12 Gauss stations
A1	Mesh	14 elements	8 elements	8 elements	8 elements
	P	420.0	530.0	530.0	530.0
	A	75.5 [-0.5816%]	167.0 [0.0632%]	166.8 [-0.0167%]	166.9 [-0.0001%]
	B	6.40 e ⁻² [-0.3611%]	8.23 e ⁻² [0.1429%]	8.23 e ⁻² [0.0411%]	8.22 e ⁻² [0.0171%]
A2	Mesh	14 elements	8 elements	8 elements	8 elements
	P	460.0	580.0	580.0	580.0
	A	87.4 [-0.3848%]	177.8 [0.0019%]	177.7 [-0.0016%]	177.7 [0.0004%]
	B	6.78e ⁻² [-0.3724%]	8.87e ⁻² [0.1001%]	8.87e ⁻² [0.0592%]	8.86e ⁻² [0.0195%]
A3	Mesh	26 elements	8 elements	8 elements	8 elements
	P	475.0	640.0	640.0	640.0
	A	50.9 [0.2658%]	124.7 [-0.1938%]	125.0 [0.0138%]	124.9 [-0.0357%]
	B	4.70e ⁻² [0.5600%]	6.13e ⁻² [-0.0514%]	6.14e ⁻² [0.0650%]	6.13e ⁻² [-0.0116%]
A4	Mesh	14 elements	8 elements	8 elements	8 elements
	P	500.0	640.0	640.0	640.0
	A	62.1 [0.1127%]	114.8 [0.1135%]	114.8 [0.0563%]	114.8 [0.0432%]
	B	4.88e ⁻² [0.3330%]	5.69e ⁻² [0.3558%]	5.68e ⁻² [0.1973%]	5.68e ⁻² [0.1525%]
A5	Mesh	14 elements	14 elements	14 elements	14 elements
	P	500.0	500.0	500.0	500.0
	A	72.8 [0.2828%]	72.8 [0.2390%]	72.7 [0.1358%]	72.6 [0.0170%]
	B	5.75e ⁻² [0.4260%]	5.76e ⁻² [0.4968%]	5.75e ⁻² [0.2993%]	5.73e ⁻² [0.0365%]
A6	Mesh	26 elements	26 elements	26 elements	8 elements
	P	450.0	450.0	450.0	550.0
	A	75.3 [-0.9438%]	75.4 [-0.8306%]	76.0 [0.0793%]	113.2 [-0.0285%]
	B	6.87e ⁻² [-0.8658%]	6.89e ⁻² [-0.5772%]	6.94e ⁻² [0.1489%]	5.72e ⁻² [-0.2627%]

For all beams, the analyses based on 12 and 24 elements (equivalent to $\psi_{LD} = 1$ and 0.5 respectively) model the experimental behaviour of the three beams very well, while the results with 6 and 2 element meshes overestimate their capacities. To remain within the $\eta = 1\%$ error of the numerical results obtained using 24 Gauss stations, 3~5 stations were needed for the 24 element discretisations, while a slightly larger number was required for the other meshes. In general, the 12 and 24 element discretisations (i.e. $\psi_{LD} = 1$ and 0.5) adequately model the behaviour of the three specimens with a minimum of 12 and 3 Gauss stations respectively. In particular, the proposed direct stiffness method was able to predict the strain distribution very well at different locations along the beam length, as depicted in Figs. 12(d), 13(c), 13(g) and 13(h).

4.5. Experiments by Ansourian (1981)

Ansourian (1981) reported a series of experiments on continuous beams, whose material and cross-

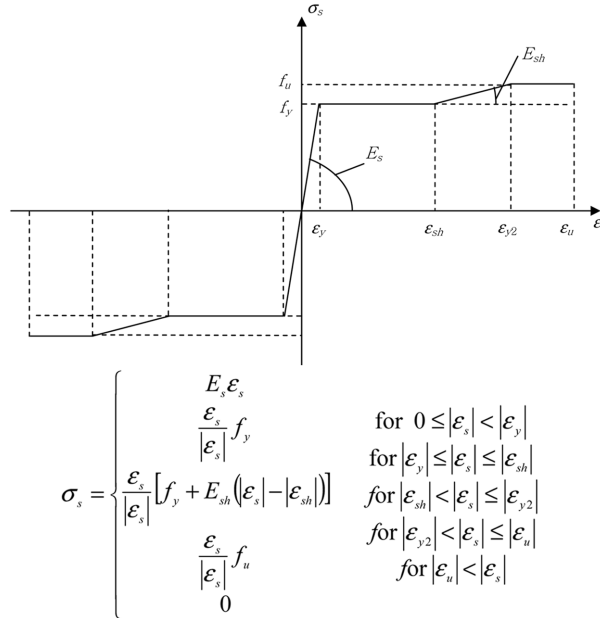


Fig. 11 Nonlinear constitutive law for the steel: quadrilinear model

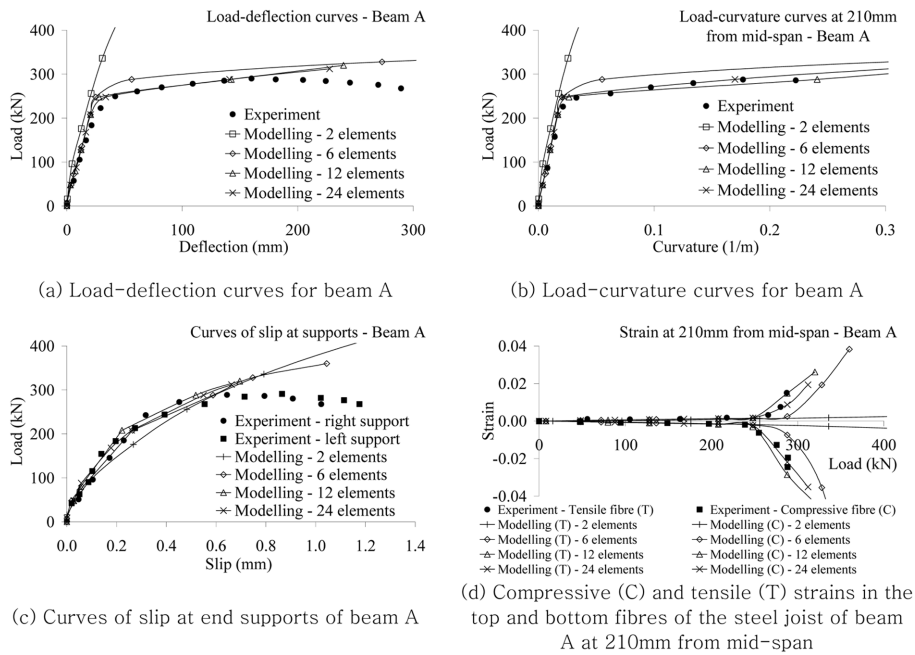


Fig. 12 Experimental results for beam A (Fabbrocino *et al.* 1998)

sectional properties were given in detail. Based on these properties that are given partly in Tables 3 and 4, the concrete was represented by the CEB-FIB modelling (1993) (Fig. 6), while the model proposed

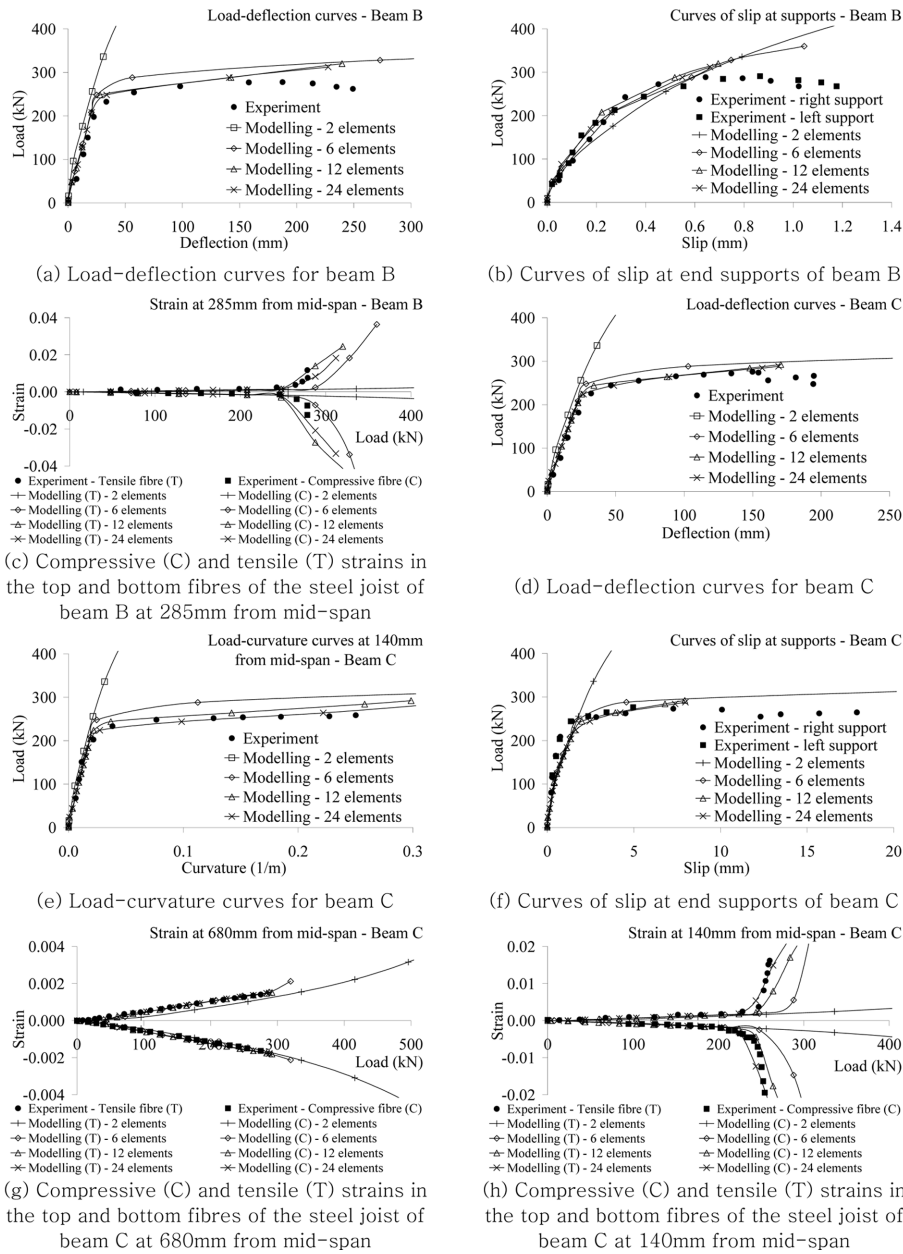


Fig. 13 Experimental results for beams B and C (Fabbrocino *et al.* 1998, 1999)

in CEB-FIB (1998) and that is reproduced in Fig. 14, was used to describe the stress-strain response of the steel joist and reinforcement. The model given in Fig. 8 was adopted for the shear connection. Similar material representations have been utilised by Zona (2003) in the simulation of these experiments. The selection of the material properties as close as possible to the experimental stress-strain curves observed for the different materials is very important in the validation process. Similarly

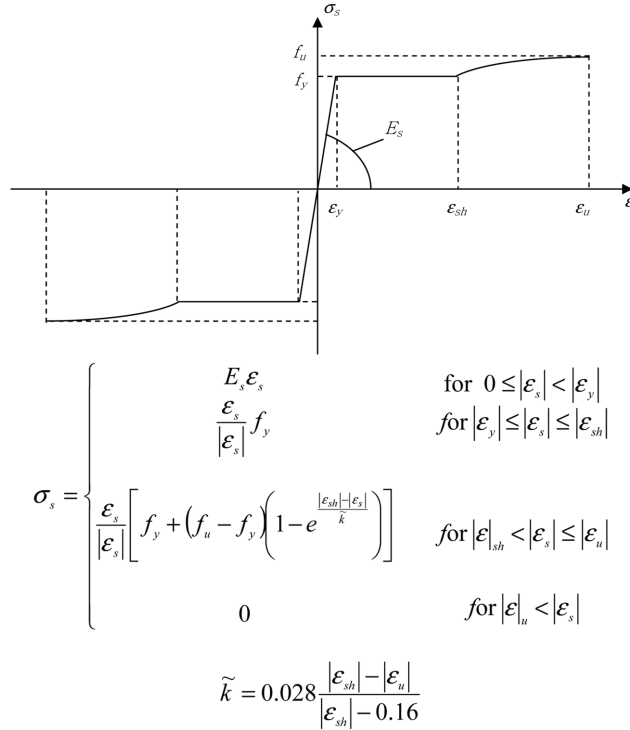


Fig. 14 Nonlinear constitutive law for the steel: model proposed in (CEB-FIB 1998)

to the hogging region tests, an adequate representation of the concrete behaviour is essential to well depict the deformation state of the composite members.

The graphical comparison (Stage 1) given in Fig. 15 for beams CTB1 and CTB2 shows that the 30 and 60 element meshing (equivalent to $\psi_{LD} = 1$ and 0.5) predicts the load-deflection curves in the sagging and hogging moment regions (in the left and right spans respectively) quite well, while modelling based on fewer elements leads to overestimates of the beam capacity (a slight overestimate with 15 elements and a large overestimate with 5 elements). For beams CTB1 and CTB2, 3 Gauss stations are adequate when discretised with 60 elements, 5 Gauss stations are adequate when discretised with 15 and 30 elements, while 24 Gauss stations are needed in the case of a 5 element discretisation to remain within the selected 1% margin.

In the case of beams CTB3 and CTB4, a meshing based on 32 and 64 elements (equivalent to element coefficients ψ_{LD} of 1 and 0.5 respectively) predict the experimental curve well, while the other meshes overestimate the beams' capacities. In these cases, 3 Gauss stations are sufficient for the meshing with 64 elements, 5 Gauss stations for 18 and 32 elements, and 24 Gauss stations for 6 elements.

For beams CTB5 and CTB6, the discretisations based on 28 and 56 elements provide good predictions of the experimental curve, but with a slight overestimation with the 16 element discretisation. The curve obtained using 6 elements overestimates the experimental one. 3 Gauss stations are sufficient for the discretisation with 56 elements, 3 to 5 with 28 elements, while 5 and 24 Gauss stations are required using 16 and 6 elements respectively.

Based on the above, the discretisation using ψ_{LD} equal to 1 and 0.5 adequately model the behaviour of the six specimens with 5 and 3 Gauss stations respectively.

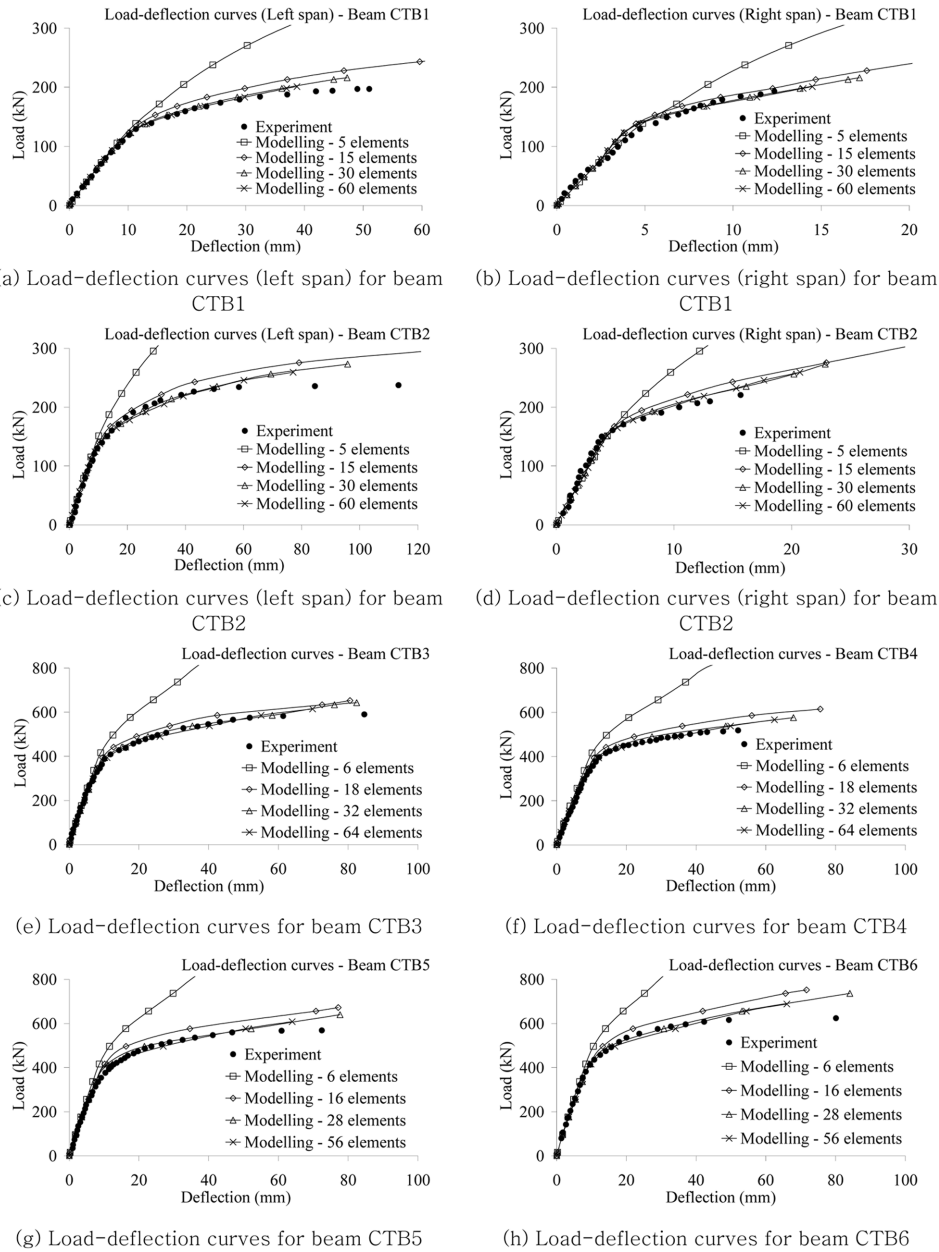


Fig. 15 Experimental results for beams CTB1, CTB2, CTB3, CTB4, CTB5 and CTB6 (Ansourian 1981)

5. Conclusions

This paper has presented a modelling technique that is able to depict the nonlinear behaviour of composite beams with partial shear interaction. The proposed approach extended the applicability of two stiffness elements, i.e. the 6DOF and the 8DOF elements, which were derived previously by the

Table 7 Nonlinear modelling results for beams reported in (Fabbrocino *et al.* 1998, 1999)

BEAM		Variable			
		3 Gauss stations	5 Gauss stations	7 Gauss stations	12 Gauss stations
P = peak load of the analysis in kN					
A = deflection at mid-span in mm at peak load [error %]					
B = curvature in 1/m calculated at 210 mm from mid-span at peak load [error %]					
C = extreme tensile strain of steel joist calculated at 210 mm from mid-span at peak load [error %]					
D = extreme compressive strain of steel joist calculated at 210 mm from mid-span at peak load [error %]					
E = curvature in 1/m calculated at 140 mm from mid-span at peak load [error %]					
F = slip in mm calculated at the supports at peak load [error %]					
G = extreme tensile strain of steel joist calculated at 680 mm from mid-span at peak load [error %]					
H = extreme compressive strain of steel joist calculated at 680 mm from mid-span at peak load [error %]					
I = extreme tensile strain of steel joist calculated at 140 mm from mid-span at peak load [error %]					
J = extreme compressive strain of steel joist calculated at 140 mm from mid-span at peak load [error %]					
Mesh		24 elements	6 elements	6 elements	6 elements
P		312.0	360.0	360.0	360.0
A	A	226.9 [-0.2975%]	658.5 [-0.1418%]	659.4 [-0.0041%]	659.6 [0.0293%]
	B	3.02e ⁻¹ [-0.2226%]	7.48e ⁻¹ [-0.1387%]	7.49e ⁻¹ [0.0018%]	7.49e ⁻¹ [0.0319%]
	C	1.93e ⁻² [-0.3059%]	3.82e ⁻² [-0.0545%]	3.83e ⁻² [0.0796%]	3.83e ⁻² [0.0266%]
	D	-3.51e ⁻² [0.1768%]	-9.64e ⁻² [0.1720%]	-9.66e ⁻² [0.0291%]	-9.66e ⁻² [-0.0340%]
Mesh		24 elements	6 elements	6 elements	6 elements
P		312.0	360.0	360.0	360.0
B	A	226.9 [-0.2975%]	658.5 [-0.1418%]	659.4 [-0.0041%]	659.6 [0.0293%]
	C	1.81e ⁻² [-0.5913%]	3.64e ⁻² [-0.0767%]	3.65e ⁻² [0.0650%]	3.64e ⁻² [0.0200%]
	D	-3.32e ⁻² [0.2976%]	-9.19e ⁻² [0.1815%]	-9.20e ⁻² [0.0353%]	-9.21e ⁻² [-0.0312%]
	Mesh		24 elements	24 elements	24 elements
P		288.0	288.0	288.0	292.0
C	A	169.2 [0.1394%]	169.5 [0.3034%]	169.3 [0.2149%]	171.3 [0.4342%]
	E	3.42e ⁻¹ [0.3312%]	3.42e ⁻¹ [0.4575%]	3.42e ⁻¹ [0.3262%]	3.00e ⁻¹ [0.5191%]
	F	8.01 [0.3370%]	8.02 [0.5144%]	8.01 [0.3671%]	8.01 [0.7758%]
	G	1.49e ⁻³ [-0.0115%]	1.49e ⁻³ [-0.0125%]	1.49e ⁻³ [-0.0089%]	-1.78e ⁻³ [0.0073%]
	H	-1.77e ⁻³ [0.0038%]	-1.77e ⁻³ [0.0041%]	-1.77e ⁻³ [0.0029%]	1.50e ⁻³ [-0.0221%]
	I	2.41e ⁻² [0.6441%]	2.42e ⁻² [0.7913%]	2.41e ⁻² [0.5642%]	-3.16e ⁻² [-0.2686%]
	J	-3.74e ⁻² [-0.1300%]	-3.74e ⁻² [-0.2430%]	-3.74e ⁻² [-0.1732%]	1.87e ⁻² [0.9923%]

authors in the linear-elastic range (Ranzi *et al.* 2004, Ranzi and Bradford 2007) to account for material nonlinearities. The elements were derived by means of the direct stiffness method, whose freedoms include the vertical displacement, the rotation and the slip at both ends for the 6DOF stiffness element, as well as the axial displacement at the level of the reference axis for the 8DOF stiffness element.

The iterative scheme of the solution strategy was based on the secant method, while the convergence criteria relied on the ratios of Euclidean norms of both forces and displacements. The main advantage of this approach is that the displacement fields of the stiffness elements considered are very rich, as they are equivalent to the analytical ones describing the elastic behaviour of the composite beams with partial interaction. The numerical formulation was found to be robust.

The proposed modelling technique has been validated against experimental data available in the literature, using the experiments reported by Chapman and Balakrishnan (1964), Fabbrocino *et al.* (1998,

Table 8 Nonlinear modelling results for beams reported in (Ansourian 1981)

BEAM	Variable	P = peak load of the analysis in kN A = deflection at mid-span (downwards in left span) in <i>mm</i> at peak load [error %] B = deflection at mid-span (downwards in left span) in <i>mm</i> at peak load [error %] C = deflection at mid-span (upwards in right span) in <i>mm</i> at peak load [error %] D = curvature in $1/m$ calculated in the sagging moment region at peak load [error %] E = curvature in $1/m$ calculated in the hogging moment region at peak load [error %]			
		3 Gauss stations	5 Gauss stations	7 Gauss stations	12 Gauss stations
CTB1	Mesh	60 elements	15 elements	15 elements	5 elements
	P	201.0	249.0	249.0	435.6
	B	38.8 [0.0746%]	66.7 [-0.1262%]	66.8 [0.0567%]	152.9 [0.0137%]
	C	$8.58e^{-2}$ [0.0003%]	$6.01e^{-2}$ [0.0962%]	$6.01e^{-2}$ [-0.0424%]	$2.65e^{-1}$ [-0.3348%]
	D	14.5 [-0.0011%]	22.1 [-0.0766%]	22.2 [0.0333%]	71.0 [-0.1065%]
	E	$1.08e^{-2}$ [0.3310%]	$2.68e^{-2}$ [-0.0033%]	$2.68e^{-2}$ [0.0868%]	$7.19e^{-2}$ [0.0053%]
CTB2	Mesh	60 elements	15 elements	15 elements	15 elements
	P	259.2	302.4	302.4	302.4
	B	76.9 [-0.2560%]	140.6 [-0.0135%]	140.7 [0.0135%]	140.7 [0.0230%]
	C	$1.51e^{-1}$ [-0.6058%]	$1.63e^{-1}$ [0.0198%]	$1.63e^{-1}$ [0.0296%]	$1.63e^{-1}$ [0.0228%]
	D	20.7 [-0.1813%]	29.6 [-0.0265%]	29.6 [-0.0650%]	29.6 [0.0357%]
	E	$2.96e^{-2}$ [-0.0966%]	$9.29e^{-2}$ [0.0053%]	$9.29e^{-2}$ [0.0014%]	$9.29e^{-2}$ [0.0681%]
CTB3	Mesh	64 elements	18 elements	18 elements	18 elements
	P	604.8	652.8	652.8	652.8
	A	63.2 [0.6998%]	80.5 [0.0088%]	80.4 [-0.1063%]	80.5 [0.0035%]
	D	$1.24e^{-1}$ [-0.9114%]	$1.42e^{-1}$ [0.0271%]	$1.42e^{-1}$ [-0.2677%]	$1.42e^{-1}$ [0.0133%]
	E	$4.75e^{-2}$ [0.6221%]	$9.00e^{-2}$ [-0.0216%]	$8.99e^{-2}$ [-0.1517%]	$9.00e^{-2}$ [0.0099%]
CTB4	Mesh	32 elements	18 elements	18 elements	18 elements
	P	576.0	614.4	604.8	614.4
	A	67.7 [-0.3347%]	75.8 [0.2377%]	67.9 [-0.0263%]	75.7 [0.1241%]
	D	$1.23e^{-1}$ [-0.2971%]	$1.42e^{-1}$ [0.0455%]	$1.34e^{-1}$ [0.0188%]	$1.42e^{-1}$ [-0.0171%]
	E	$1.02e^{-1}$ [-0.3831%]	$8.17e^{-2}$ [0.3079%]	$7.30e^{-2}$ [0.0017%]	$8.16e^{-2}$ [0.1365%]
CTB5	Mesh	28 elements	16 elements	16 elements	16 elements
	P	640.0	672.0	672.0	672.0
	A	77.3 [-0.5164%]	77.2 [0.0667%]	77.2 [0.0545%]	77.2 [0.0403%]
	D	$1.32e^{-1}$ [-0.6264%]	$1.33e^{-1}$ [0.0472%]	$1.33e^{-1}$ [0.0269%]	$1.33e^{-1}$ [0.0219%]
	E	$1.09e^{-1}$ [-0.6744%]	$7.51e^{-2}$ [0.1040%]	$7.51e^{-2}$ [0.0765%]	$7.51e^{-2}$ [0.0527%]
CTB6	Mesh	56 elements	16 elements	16 elements	16 elements
	P	688.0	752.0	752.0	752.0
	A	65.9 [-0.2397%]	71.7 [0.0205%]	71.7 [0.0006%]	71.7 [0.0053%]
	D	$1.19e^{-1}$ [-0.4064%]	$1.26e^{-1}$ [0.1003%]	$1.26e^{-1}$ [0.0035%]	$1.26e^{-1}$ [-0.0023%]
	E	$1.27e^{-1}$ [0.2776%]	$6.96e^{-2}$ [0.0602%]	$6.95e^{-2}$ [0.0064%]	$6.95e^{-2}$ [-0.0077%]

1999) and Ansourian (1981). These consist of six simply supported beams with a point load applied at mid span inducing positive bending moment in the beams, three simply supported beams with a point

load applied at mid span inducing negative bending moment in the beams, and six two-span continuous composite beams respectively.

Based on the parametric studies and numerical considerations given in the validation process, it can be concluded that the nonlinear modelling technique based on the direct stiffness approach is able to describe the nonlinear behaviour of composite beams with partial interaction very well if the discretisation based on an element whose length to depth ratio $\psi_{L/D}$ is in the approximate range 0.5~1.0. In this case, 3~5 Gauss stations are needed. Coarser discretisations may require significantly larger numbers of Gauss stations, and the recommendation from the study is that optimal and accurate numerical modelling of the nonlinear response of composite beams based on the direct stiffness approach is achieved with a meshing with $\psi_{L/D} = 0.5$ and with 5 Gauss stations per element.

Acknowledgements

The work in this paper was supported in part by the Australian Academy of Science and the Australian Research Council.

References

- ABAQUS (2003), *ABAQUS Standard User's Manual, Version 6.4*, Hibbit, Karlsson and Sorensen Inc., Pawtucket, RI, USA.
- Ansourian, P. (1981), "Experiments on continuous composite beams", *Proc. Inst. Civil Eng., London*, Part 2, **71**, 25-51.
- Ansys (2003), *Ansys Multiphysics 8.0*, Ansys Inc., Canonsburg, Pa, USA.
- CEB-FIB (Comité Euro-International du Béton - Fédération International de la Précontrainte) (1993), *Model Code 1990: Design Code*, Thomas Telford, London, UK.
- CEB-FIB (Comité Euro-International du Béton - Fédération International de la Précontrainte) (1998), *CEB Bulletin d'information n. 242: Ductility of reinforced concrete structures*, FIB Fédération International du Béton, Paris, France, 112-113.
- Chapman, J.C. and Balakrishnan, S. (1964), "Experiments on composite beams", *The Structural Engineer*, **42**(11), 369-383.
- Faella, C., Martinelli, E. and Nigro, E. (2002), "Steel and concrete composite beams with flexible shear connection: "exact" analytical expression of the stiffness matrix and applications", *Comput. Struct.*, **80**, 1001-1009.
- Faella, C., Martinelli, E. and Nigro, E. (2003), "Shear connection nonlinearity and deflections of steel-concrete composite beams: A simplified method", *J. Struct. Eng.*, ASCE, **129**(1), 12-20.
- Fabbrocino, G., Manfredi, G., Pecce, M. and Cosenza, E. (1998), "Nonlinear behaviour of composite beams in the hogging moment region: numerical study", *Proc. III Italian Workshop on Composite Construction*, Ancona, Italy, October 1998 (In Italian).
- Fabbrocino, G., Manfredi, G., Cosenza, E. and Pecce, M. (1999), "Nonlinear behaviour of composite beams under negative moment: an experimental-theoretical comparison", *Proc. of the 2nd European Conf. Steel Structures EUROSTEEL '99*, Prague, Czech Republic, May 1999.
- Girhammar, U.A. and Pan, D. (1993), "Dynamic analysis of composite members with interlayer slip", *Int. J. Solids Struct.*, **30**(6), 797-823.
- Leon, R.T. and Viest, I.M. (1996), "Theories of incomplete interaction in composite beams", *Proc. Conf. Comp. Constr. Steel. Con. III*, Irsee, Germany, June, 858-870.
- May, I.M., Morley, C.T. and Chen, Y.Y. (2003), "Benchmarking of non-linear finite element analyses for reinforced concrete deep beams", *Proc. EURO-C 2003 Conf. Computational Modelling of Concrete Structures*, St. Johann

- im Pongau, Austria, 751-756.
- Newmark, N.M., Siess, C.P. and Viest, I.M. (1951), "Tests and analysis of composite beams with incomplete interaction", *Proc. Society Experimental Stress Analysis*, **9**(1), 75-92.
- Pi, Y. L., Bradford, M.A. and Uy, B. (2005a), "Second-order nonlinear inelastic analysis of composite steel-concrete composite members. I: Theory", *J. Struct. Eng.*, ASCE, **132**(5), 751-761.
- Pi, Y. L., Bradford, M.A. and Uy, B. (2005b), "Second-order nonlinear inelastic analysis of composite steel-concrete composite members. II: Applications", *J. Struct. Eng.*, ASCE, **132**(5), 762-771.
- Ranzi, G. and Bradford, M.A. (2007), "Direct stiffness analysis of a composite beam-column element with partial interaction", *Comput. Struct.* (accepted for publication).
- Ranzi, G., Bradford, M.A. and Uy, B. (2003), "A general method of analysis of composite beams with partial interaction", *Steel Composite Struct.*, **3**(3), 169-184.
- Ranzi, G., Bradford, M.A. and Uy, B. (2004), "A direct stiffness analysis of a composite beam with partial interaction", *Int. J. Numer. Meth. Eng.*, **61**, 657-672.
- Reddy, J.N. (2004), *An Introduction to Nonlinear Finite Element Analysis*, Oxford University Press, Oxford, UK.
- Spacone, E. and El-Tawil, S. (2004), "Nonlinear analysis of steel-concrete composite structures: state of the art", *J. Struct. Eng.*, ASCE, **130**(2), 159-168.
- Sun, C.H., Bradford, M.A. and Gilbert, R.I. (1993), "Numerical analysis for concrete framed structures using the finite element method", *Comput. Struct.*, **48**(1), 73-79.
- Weaver, W. and Gere, J.M. (1990), *Matrix Analysis of Framed Structures*, 3rd edn., Chapman and Hall, London, 1990.
- Yam, L.C.P. and Chapman, J.C. (1968), "The inelastic behaviour of simply supported composite beams of steel and concrete", *Proc. of the Institution of Civil Engineers, London*, Part 2, **41**, 651-683.
- Zhang, Y.X., Bradford, M.A. and Gilbert, R.I. (2006), "A new triangular layered plate element for the nonlinear analysis of reinforced concrete slabs", *Commun. Numer. Meth. Eng.*, **22**(7), 677-709.
- Zona, A. (2003), "Finite Element Modelling of Composite Beams", PhD Thesis, University of Ancona, Italy.

BU

APPENDIX

A_c, A_r, A_s = area of concrete component, reinforcement and steel joist respectively

$$A\tilde{E}_1 = A_c E_c + A_r E_r ; A\tilde{E}_2 = A_s E_s ; A\tilde{E} = A\tilde{E}_1 + A\tilde{E}_2$$

B_c, B_r, B_s = first moment of area of concrete component, reinforcement and steel joist respectively, calculated about the arbitrary reference axis

$$B\tilde{E}_1 = B_c E_c + B_r E_r ; B\tilde{E}_2 = B_s E_s ; B\tilde{E} = B\tilde{E}_1 + B\tilde{E}_2$$

$$b_1 = \frac{B\tilde{E} + y_0 A\tilde{E}}{A\tilde{E}I\tilde{E} - B\tilde{E}^2} ; b_2 = \frac{y_0 B\tilde{E} + I\tilde{E}}{A\tilde{E}I\tilde{E} - B\tilde{E}^2}$$

$$b_3 = \frac{B\tilde{E}B\tilde{E}_2 + y_0(B\tilde{E}_2 A\tilde{E}_1 - B\tilde{E}_1 A\tilde{E}_2) - A\tilde{E}_2 I\tilde{E}}{A\tilde{E}I\tilde{E} - B\tilde{E}^2}$$

E_c, E_r, E_s = secant modulus of concrete component, reinforcement and steel joist respectively

I_c, I_r, I_s = second moment of area of concrete component, reinforcement and steel joist respectively, calculated about the arbitrary reference axis

$$I\tilde{E}_1 = I_c E_c + I_r E_r ; I\tilde{E}_2 = I_s E_s ; I\tilde{E} = I\tilde{E}_1 + I\tilde{E}_2$$

$$r_1 = -\frac{A\tilde{E}}{A\tilde{E}I\tilde{E} - B\tilde{E}^2} ; r_2 = \frac{-B\tilde{E}}{A\tilde{E}I\tilde{E} - B\tilde{E}^2} ; r_3 = \alpha$$

$$q_1 = \frac{B\tilde{E}_1 A\tilde{E}_2 - B\tilde{E}_2 A\tilde{E}_1}{A\tilde{E}I\tilde{E} - B\tilde{E}^2} ; q_2 = \frac{A\tilde{E}_1 I\tilde{E} - B\tilde{E}_1 B\tilde{E}}{A\tilde{E}I\tilde{E} - B\tilde{E}^2} ; q_3 = \frac{B\tilde{E}_1^2 A\tilde{E}_2 + B\tilde{E}_2^2 A\tilde{E}_1 - I\tilde{E} A\tilde{E}_1 A\tilde{E}_2}{A\tilde{E}I\tilde{E} - B\tilde{E}^2}$$

$$\tilde{\alpha} = \frac{B\tilde{E}_1^2 A\tilde{E}_2 + B\tilde{E}_2^2 A\tilde{E}_1 - I\tilde{E} A\tilde{E}_1 A\tilde{E}_2}{A\tilde{E}I\tilde{E} - B\tilde{E}^2} ; \alpha = \frac{B\tilde{E}_1 A\tilde{E}_2 - B\tilde{E}_2 A\tilde{E}_1}{A\tilde{E}I\tilde{E} - B\tilde{E}^2} ; \alpha_1 = \frac{A\tilde{E}_1 I\tilde{E} - B\tilde{E}_1 B\tilde{E}}{A\tilde{E}I\tilde{E} - B\tilde{E}^2} ; \mu^2 = \frac{k}{\tilde{\alpha}}$$

$$A\tilde{E}_{S1.m.li} = \sum_{g=1}^{g_{\max}} w_g \sum_{j=1}^{j_{\max 1}} A_{m.gj} E_{m.ligj} ; A\tilde{E}_{S2.m.li} = \sum_{g=1}^{g_{\max}} w_g \sum_{j=j_{\max 1}+1}^{j_{\max 2}} A_{m.gj} E_{m.ligj}$$

$$B\tilde{E}_{S1.m.li} = \sum_{g=1}^{g_{\max}} w_g \sum_{j=1}^{j_{\max 1}} y_{m.gj} A_{m.gj} E_{m.ligj} ; B\tilde{E}_{S2.m.li} = \sum_{g=1}^{g_{\max}} w_g \sum_{j=j_{\max 1}+1}^{j_{\max 2}} y_{m.gj} A_{m.gj} E_{m.ligj}$$

$$I\tilde{E}_{S1.m.li} = \sum_{g=1}^{g_{\max}} w_g \sum_{j=1}^{j_{\max 1}} y_{m.gj}^2 A_{m.gj} E_{m.ligj} ; I\tilde{E}_{S2.m.li} = \sum_{g=1}^{g_{\max}} w_g \sum_{j=j_{\max 1}+1}^{j_{\max 2}} y_{m.gj}^2 A_{m.gj} E_{m.ligj}$$

$$A\tilde{E}_{S.m.li} = A\tilde{E}_{S1.m.li} + A\tilde{E}_{S2.m.li} ; B\tilde{E}_{S.m.li} = B\tilde{E}_{S1.m.li} + B\tilde{E}_{S2.m.li}$$

$$I\tilde{E}_{S.m.li} = I\tilde{E}_{S1.m.li} + I\tilde{E}_{S2.m.li} ; k_{S.m.li} = \sum_{g=1}^{g_{\max}} w_g k_{S.m.lig}$$